

# RSC Advances

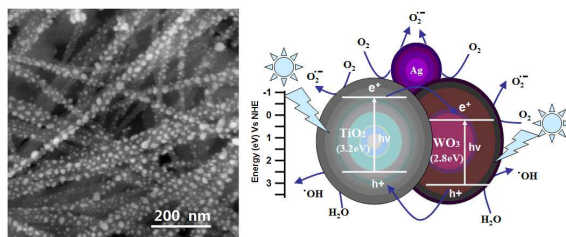


This is an *Accepted Manuscript*, which has been through the Royal Society of Chemistry peer review process and has been accepted for publication.

*Accepted Manuscripts* are published online shortly after acceptance, before technical editing, formatting and proof reading. Using this free service, authors can make their results available to the community, in citable form, before we publish the edited article. This *Accepted Manuscript* will be replaced by the edited, formatted and paginated article as soon as this is available.

You can find more information about *Accepted Manuscripts* in the [Information for Authors](#).

Please note that technical editing may introduce minor changes to the text and/or graphics, which may alter content. The journal's standard [Terms & Conditions](#) and the [Ethical guidelines](#) still apply. In no event shall the Royal Society of Chemistry be held responsible for any errors or omissions in this *Accepted Manuscript* or any consequences arising from the use of any information it contains.



TiO<sub>2</sub> nanowires decorated with Ag and WO<sub>3</sub> nanoparticles and the schematic diagram of charge carriers' separation in Ag-WO<sub>3</sub>/TiO<sub>2</sub> photocatalyst.

## WO<sub>3</sub> and Ag nanoparticles co-sensitized TiO<sub>2</sub> nanowires: preparation and the enhancement of photocatalytic activity

Yang Li<sup>a,b</sup>, Wenjian Wu<sup>a</sup>, Peng Dai<sup>a</sup>, Lili Zhang<sup>a</sup>, Zhaoqi Sun<sup>a</sup>, Guang Li<sup>a</sup>, Mingzai Wu<sup>\*a</sup>,  
Xiaoshuang Chen<sup>c</sup>, Changle Chen<sup>\*d</sup>

- <sup>a)</sup> School of Physics and Materials Science, Anhui University, Hefei 230039, P.R.China  
<sup>b)</sup> School of Science, Anhui University of Science and Technology, Huainan 232001, P.R.China  
<sup>c)</sup> Shanghai Institute of Technical Physics of the Chinese Academy of Sciences, Shanghai 200083, P.R.China  
<sup>d)</sup> CAS Key Laboratory of Soft Matter Chemistry, Department of Polymer Science and Engineering, University of Science and Technology of China, Hefei, 230026, China

**Abstract:** In this paper, TiO<sub>2</sub> nanowires decorated with WO<sub>3</sub> nanoparticles (WO<sub>3</sub>-TWS) on Ti foils were prepared using simple hydrothermal treatment, wet impregnation and subsequent annealing treatment sequentially. Ag nanoparticles were successfully deposited on the obtained WO<sub>3</sub>-TWS by successive ionic layer adsorption reaction technique. Ultraviolet-visible absorption spectra showed that the introduction of Ag and WO<sub>3</sub> particles on TiO<sub>2</sub> nanowires surfaces extends the absorption edge to visible light regime. More importantly, the increase of Ag content greatly enhances the absorption intensity in visible light regime. The photocatalytic experiment results revealed that TiO<sub>2</sub> nanowires decorated with Ag and WO<sub>3</sub> nanoparticles possess higher photocatalytic activities toward methyl orange than pure TiO<sub>2</sub> nanowires. The degradation percentage of 95.6% after 10 cycles indicated that the as-prepared photocatalyst composites exhibited excellent long-time recyclable ability for the degradation of contaminants.

**Keywords:** Hydrothermal; TiO<sub>2</sub>; Photocatalytic activity

### 1. Introduction

Titania (titanium dioxide, TiO<sub>2</sub>) has attracted tremendous attentions as a semiconductor photocatalyst in the past decades due to its chemical stability, low cost, high reusability and excellent degradation activity of organic pollutants.<sup>1-7</sup> However, some issues have hampered its large-scale application. For example, the wide band gap ( $E_g = 3.2$  eV) indicates that it can only be excited by ultraviolet light. The low electron transfer rate to oxygen and high

---

mingzaiwu@gmail.com (M. Wu); changle@ustc.edu.cn (C. Chen).

recombination rate between photogenerated electrons and holes greatly limit its catalytic activity.<sup>5,8,9</sup> Many efforts have been made to address these problems, including semiconductor multiplicity, nonmetal and metal doping and surface modification.<sup>10-15</sup> For example, the deposition of p-type CdS on TiO<sub>2</sub> surface was reported to greatly enhance the photocatalytic activity because the p-n heterojunction formed at the interface of CdS and TiO<sub>2</sub> effectively suppresses the recombination of photogenerated electron-hole pairs.<sup>16</sup> The doping of carbon and nitrogen was reported to extend the photoexcitation wavelength to the visible range for C-N-TiO<sub>2</sub> composite.<sup>17</sup> Surface modification with Pt was shown to enhance photogenerated charge pairs separation efficiency because metal Pt has a high work function and can easily trap the photogenerated electrons.<sup>18</sup>

Among these approaches, the formation of semiconductor heterostructures with regulated band gap is an effective way to enhance the efficiency of the photoinduced charges separation.<sup>19</sup> Recently, tungsten trioxide (WO<sub>3</sub>) has attracted much attention due to its similar ionic radius of W<sup>6+</sup> (0.740 Å) to that of Ti<sup>4+</sup> (0.745 Å), its small band gap (2.4eV-2.8eV), strong absorption of solar spectrum, and high chemical stability over a wide pH range. In addition, the W-O-Ti bond formed in WO<sub>3</sub> doped TiO<sub>2</sub>, i.e., W<sub>x</sub>Ti<sub>1-x</sub>O<sub>2</sub>, was proposed to be responsible for the narrowing of band gap in W<sub>x</sub>Ti<sub>1-x</sub>O<sub>2</sub>.<sup>20,21</sup> Over the past few years, the deposition of WO<sub>3</sub> on TiO<sub>2</sub> has been reported to extend the absorption edge to 560 nm and increase the photocatalytic percentage, which is still far from the visible light absorption edge.<sup>22</sup>

Due to surface Plasmon resonance effect, silver nanoparticles have shown great potentials in photochemical fields due to its highly adjustable absorption. It has been reported that the introduction of silver particles to TiO<sub>2</sub> nanostructures could improve the absorbance, and extended the absorption to almost whole visible light range.<sup>23-26</sup> Moreover, the deposition of noble metal on the surface of TiO<sub>2</sub> can serve as a sink for charge carriers, promote interfacial charge transfer and inhibit recombination of photogenerated electron-hole pairs.<sup>27-29</sup> Despite these achievements, the exploration of photocatalyst with high photodegradation percentages, low cost, no second pollution and recyclability is still highly desired.

In this paper, we presented the preparation of TiO<sub>2</sub> nanowires on Ti foils decorated with

WO<sub>3</sub> and Ag particles via hydrothermal treatment, wet impregnation and successive ionic layer adsorption reaction (SILAR) technique. The as-prepared composite photocatalysts (Ag-WO<sub>3</sub>-TWS) showed greatly improved absorbance even in the infrared regime and dramatically improved photocatalytic activities toward methyl orange degradation than that of TiO<sub>2</sub> nanowires. In addition, the as-prepared Ag-WO<sub>3</sub>-TWS composite exhibited excellent recyclability for pollutants degradation.

## 2. Experimental section

### 2.1 Synthesis of Ag-WO<sub>3</sub>-TWS photocatalysts

All chemicals are of analytical grade and used as received. In a typical synthesis: Ti foils were cut into 12 mm×10 mm in size and ultrasonically cleaned in acetone, alcohol and distilled water for 5 min, respectively. After polishing in a mixed solution of HF, HNO<sub>3</sub> and distilled water (the volume ratio is 1:1:4) for 10 min, 30 mL of 1M NaOH aqueous solution and the polished Ti foils were transferred into a 50 ml Teflon-lined autoclave, which were kept at 200 °C for 48 h before cooling to room temperature naturally. The processed foils were rinsed thoroughly with distilled water and ethanol. WO<sub>3</sub>-TWS were prepared via wet impregnation using ammonium paratungstate (APT) as the precursor. The foils containing TiO<sub>2</sub> nanowires were dipped into 0.1 M APT aqueous solution for 3 h and then dried with a stream of N<sub>2</sub>. Subsequently, the samples were annealed at 500 °C in an argon atmosphere for 3 h. For the preparation of Ag-WO<sub>3</sub>-TWS photocatalysts, the obtained WO<sub>3</sub>-TWS was immersed in 20 mL AgNO<sub>3</sub> aqueous solution (4 mM) for 5 min, and subsequently immersed in 20 mL NaBH<sub>4</sub> aqueous solution (2 mM) for 5 more min. Then, the obtained sample was dried at room temperature and labeled as Ag(1)-0.1M WO<sub>3</sub>-TWS. Similar experimental procedures were performed with other parameters unchanged except the APT concentration and repetitive times of the immersion process. The samples labeled as Ag(3)-0.05M WO<sub>3</sub>-TWS and Ag(5)-0.05M WO<sub>3</sub>-TWS correspond to 3 and 5 times of immersion, respectively.

### 2.2 Characterization

The structures and morphologies of the as-obtained samples were characterized by X-ray powder diffraction (XRD, Bruker D8-ADVANCE) using an 18 kW advanced X-ray

diffractometer with Cu K $\alpha$  radiation ( $\lambda=1.54056 \text{ \AA}$ ), scanning electron microscopy (FESEM, FEI Sirion 200) and high resolution transmission electron microscopy (HRTEM, JEOL-2010). Ultraviolet-visible absorption spectra (UV-vis) were measured using a U-4100 Hitachi Ultraviolet-Visible-Near-Infrared spectrophotometer in the range of 240 to 800 nm. X-ray photoelectron spectroscopy (XPS, Thermo, ESCALAB250) was employed to analyze the surface compositions and chemical state of the samples.

### 2.3 Photocatalytic experimental details

The photocatalytic degradation experiments toward methyl orange were carried out in a self-prepared reactor. In the degradation procedure, samples were immersed in a 25 mL beaker containing 20 mL of methyl orange aqueous solution (15 mg/L). Before irradiation by a 350 W Xenon lamp (XQ350W, Lansheng electronics co., LTD, Shanghai, China), adsorption equilibrium of the dye molecules on catalyst surface was established by stirring in the dark for 30 min and the vertical distance between the solution level and the horizontal plane of the lamp was fixed at 10 cm (The excitation power density is  $160 \text{ mW/cm}^2$ ). Upon irradiation, 0.5 mL of oxydol solution (30%, m/v) was added to the beaker, and the methyl orange aqueous solution was kept being stirred. At an interval of 10 min, 3 mL of solution is taken out from the reactor. The absorbance of the solution was determined on a UV-Vis absorption photometer (UV-3200S, MAPADA analytic apparatus Ltd. Inc., Shanghai, China) at 464 nm wavelength. The visible light source was obtained using a 420 nm cutoff filter in the experiment (The excitation power density is  $118 \text{ mW/cm}^2$ ).

## 3. Results and discussion

XRD patterns of WO $_3$ -TWS samples are shown in Fig. 1a. For sample 0.01 M WO $_3$ -TWS, all diffraction peaks can be indexed to Ti (JCPDS 44-1294) and anatase TiO $_2$  (JCPDS 21-1272). No peaks of WO $_3$  were found. With the increase of APT concentration to be 0.05M, peaks of WO $_3$  turn up vaguely for 0.05M WO $_3$ -TWS. When the APT concentration was increased to be 0.1M, peaks of WO $_3$  (JCPDS 43-1035) are detected. Moreover, higher APT concentration favors the formation of WO $_3$  phase on the surface of TiO $_2$ , which reduce the diffraction of inner anatase TiO $_2$  and Ti. Fig. 1b shows the XRD patterns of Ag(i)-0.05M WO $_3$ -TWS (i=1, 3, 5). Due to the low APT concentration, WO $_3$  phase is not found. When the

immersion process is performed once, peaks of silver are vague. For Ag(2)-0.05M WO<sub>3</sub>-TWS, face-centered-cubic (fcc) Ag (JCPDS 4-0783) can be indexed. With the increase of the immersion times, the relative peak intensity of Ag to TiO<sub>2</sub> is increased. The crystalline size of Ag nanoparticles for Ag(3)-0.05M WO<sub>3</sub>-TWS were estimated to be 20 nm based on the Scherrer's equation using (200) reflections.

XPS measurements were conducted for surface analysis of TiO<sub>2</sub> nanowires, 0.05 M WO<sub>3</sub>-TWS and Ag(3)-0.05 M WO<sub>3</sub>-TWS samples (Fig. 2). The detection of W4f and Ag3d peaks indicates the successful deposition. XPS spectra of Ti element for the selected samples are presented in Fig. 3a. For pure TiO<sub>2</sub> nanowires, two peaks of Ti 2p located at 458.7 eV and 464.5 eV are assigned to Ti 2p<sub>3/2</sub> and Ti 2p<sub>1/2</sub>, respectively, which agree with previously reported XPS data and can be assigned to Ti<sup>4+</sup> in pure TiO<sub>2</sub> nanowires.<sup>30</sup> Compared with pure TiO<sub>2</sub> nanowires, Ti peaks of both 0.05 M WO<sub>3</sub>-TWS and Ag(3)-0.05 M WO<sub>3</sub>-TWS are clearly blue-shifted to 459.1 eV and 464.8 eV. The O1s peak of TiO<sub>2</sub> nanowires is located at 529.8eV (Fig. 2b); while the O1s peaks of 0.05 M WO<sub>3</sub>-TWS and Ag(3)-0.05 M WO<sub>3</sub>-TWS are slightly shift to 530.3eV. The positive shift of both Ti 2P and O1s implies the possible formation of W-O-Ti linkage in the TiO<sub>2</sub> lattice.<sup>22,30</sup> The W 4f<sub>5/2</sub> and W 4f<sub>7/2</sub> peaks of both 0.05 M WO<sub>3</sub>-TWS and Ag(3)-0.05 M WO<sub>3</sub>-TWS are 36.0 eV and 37.9 eV with intensity ratio of 3:4 (Fig. 2c), consistent with the reported values for WO<sub>3</sub>.<sup>27</sup> The same peaks' positions for the two samples indicate that Ag deposition does not affect the chemical state of WO<sub>3</sub>. The Ag 3d<sub>3/2</sub> and Ag 3d<sub>5/2</sub> peaks are located at 368.1 eV and 374.3 eV (Fig.2d), which can be ascribed to metallic silver.<sup>23</sup>

Fig. 3 shows the SEM images of pure TiO<sub>2</sub> nanowires, 0.05 M WO<sub>3</sub>-TWS, Ag(i)-0.05 M WO<sub>3</sub>-TWS (i=1,3,5) and energy dispersive spectrum (EDS) images of 0.05 M WO<sub>3</sub>-TWS and Ag(3)-0.05 M WO<sub>3</sub>-TWS. The surface of titanium foil was etched and covered with TiO<sub>2</sub> nanowires with diameter of ca. 20 nm (Fig. 3a). Moreover, the TiO<sub>2</sub> nanowires possess smooth surface (Fig. 3a). After being immersed in APT aqueous solution for 2 h, the diameters remain unchanged (Fig. 3b), which imply that the deposition dosage is minute. In fact, the ionic radius of W<sup>6+</sup> (0.740Å) is slightly smaller than that of Ti<sup>4+</sup> (0.745 Å), suggesting the possibility of the substitution of Ti<sup>4+</sup> in TiO<sub>2</sub> lattice by W<sup>6+</sup> ions. After being immersed in AgNO<sub>3</sub> and NaBH<sub>4</sub> aqueous solution, the size and overall shapes of the samples

are not changed, and the deposited Ag nanoparticles on the surface of the TiO<sub>2</sub> nanowires can be observed (Fig. 3c, d, e). For sample Ag(1)-0.05 M WO<sub>3</sub>-TWS, Ag nanoparticles with sizes about 5 nm are sparsely distributed, as shown in Fig. 3c; while for sample Ag(3)-0.05 M WO<sub>3</sub>-TWS, a great numbers of Ag nanoparticles with diameters in the range of 10 to 20 nm are evenly loaded on the surface of the WO<sub>3</sub>-TWS (Fig. 3d). After immersion cycles for 5 times, Ag nanoparticles became larger, and the sizes are no longer monodisperse (Fig. 3e), resulting in sample Ag(5)-0.05 M WO<sub>3</sub>-TWS. The EDS spectra of sample 0.05 M WO<sub>3</sub>-TWS and Ag(3)-0.05 M WO<sub>3</sub>-TWS are shown in Fig. 3f. The characteristic peaks of Ti, O, W and Ti, O, W, Ag are detected, suggesting the formation of WO<sub>3</sub> and Ag-WO<sub>3</sub> nanocrystals on the TiO<sub>2</sub> nanowires.

To further investigate the microstructure of the composites, HRTEM measurements were performed on the as-obtained products scrapped off the titanium foils. Fig. 4a shows the HRTEM image of sample 0.05 M WO<sub>3</sub>-TWS. WO<sub>3</sub> nanoparticles with sizes about 1-2 nm are distributed on TiO<sub>2</sub> nanowires surfaces, making the TiO<sub>2</sub> nanowires surface rough. This can be further confirmed by the lattice fringes (Fig. 4b) of the circular area marked in Fig. 4a. The interplanar spacing are 0.35 nm and 0.524 nm (Fig. 4b), consistent with the (101) plane of anatase TiO<sub>2</sub> and (110) plane of WO<sub>3</sub>. HRTEM image of sample Ag(3)-0.05 M WO<sub>3</sub>-TWS is shown in Fig. 4c. Clearly, spherical Ag nanoparticles with diameter about 10 nm were deposited on the surface of TiO<sub>2</sub> nanowires. Fig. 4d and 4e show the lattice fringes of the boxed area and circular area marked in Fig. 4c. The spacing of the lattice planes are 0.20 nm, 0.35 nm and 0.524nm, consistent with the (200) plane of face center cubic (fcc) Ag, (101) plane of anatase TiO<sub>2</sub> and (110) plane WO<sub>3</sub> respectively.

Fig. 5 shows the UV-vis diffuse reflection absorption spectra of the as-prepared pure TiO<sub>2</sub> naowires, WO<sub>3</sub>-TWS and Ag(i)-0.05 M WO<sub>3</sub>-TWS(i=1,3,5). The absorption edges of WO<sub>3</sub>-TWS showed obvious red-shift compared with pure TiO<sub>2</sub> naowires, which might originates from the combinational effect of the narrow band gap of WO<sub>3</sub> and wide band gap of TiO<sub>2</sub>. In addition, with the increase of the WO<sub>3</sub> concentration, the absorbance in visible light zone is increased (Fig. 5a). All of the samples Ag(i)-0.05 M WO<sub>3</sub>-TWS(i=1,3,5) (Fig. 5b) possess an additional strong absorption band ranging from 450 nm to 750 nm, which are attributed to the surface plasmon resonance effect of Ag nanoparticles deposited on the

surface of the TiO<sub>2</sub> nanowires. The introduction of Ag and WO<sub>3</sub> particles on TiO<sub>2</sub> nanowires surfaces extends the absorption edge to the visible light range. More importantly, the increase of Ag content greatly enhances the absorption intensity in visible light range. Both factors are vital to the improvement of the photocatalytic activity of TiO<sub>2</sub>.<sup>25,26</sup>

The photocatalytic activities evaluation of the as-prepared samples were carried out by the degradation of methylene blue (MB) solution under Xenon lamp irradiation and the experimental results are shown in Fig. 6. The photodegradation percentages for pure TiO<sub>2</sub> nanowires, 0.01M WO<sub>3</sub>-TWS, 0.05M WO<sub>3</sub>-TWS and 0.1M WO<sub>3</sub>-TWS under simulated solar irradiation are 42.91, 47.04, 78.13 and 72.01%, respectively after 90 min irradiation, as shown in Fig. 6a. Clearly, the introduction of WO<sub>3</sub> particles on TiO<sub>2</sub> nanowires increases the photodegradation percentages. However, higher WO<sub>3</sub> concentration does not necessarily lead to higher photodegradation percentage. Because higher WO<sub>3</sub> deposition would cover more surface area of TiO<sub>2</sub> nanowires, and hence reduce the photocatalytic activity of TiO<sub>2</sub> nanowires in the ultraviolet light range. Fig. 6b shows the photodegradation percentages curves of pure TiO<sub>2</sub> nanowires, 0.01M WO<sub>3</sub>-TWS, 0.05M WO<sub>3</sub>-TWS and 0.1M WO<sub>3</sub>-TWS under visible light irradiation obtained with a 420 nm cutoff filter. In this case, the percentages are 2.95, 8.57, 34.02, 36.47% after 90 min irradiation, respectively. Under visible irradiation, the photocatalytic activities are greatly reduced and almost no activity can be detected for pure TiO<sub>2</sub> nanowires. Importantly, the differences are much more obvious between simulated solar irradiation and visible irradiation. The time-dependent photodegradation percentage of Ag(i)-0.05 M WO<sub>3</sub>-TWS(i=1,3,5) under simulated solar irradiation (Fig. 6c) and visible irradiation (Fig. 6d) were also studied. Under simulated solar irradiation after 90 min, the degradation rates of methyl orange are 92.06, 95.84 and 99.61% for Ag(1)-0.05 M WO<sub>3</sub>-TWS, Ag(3)-0.05 M WO<sub>3</sub>-TWS, and Ag(5)-0.05 M WO<sub>3</sub>-TWS, respectively. Clearly, the deposition of Ag particles further improves the photocatalytic activity. Similarly, higher Ag loadings do not necessarily result in higher photodegradation percentages. There is an optimal immersion times for these samples and Ag(3)-0.05 M WO<sub>3</sub>-TWS is the best for this case. In fact, there has been related report that high dosage of Ag nanoparticles deposited on the TiO<sub>2</sub> surface would serve as trapping centre for the photogenerated electron and holes and hence reduce the photodegradation activity.<sup>25,28</sup>

Fig. 6d shows the time-dependent photodegradation percentage curve under visible irradiation. After 90 min, the degradation rates of methyl orange are 50.45, 66.75 and 57.64% for Ag(1)-0.05 M WO<sub>3</sub>-TWS, Ag(3)-0.05 M WO<sub>3</sub>-TWS, and Ag(5)-0.05 M WO<sub>3</sub>-TWS, respectively. Compared with the simulated solar irradiation, the reduction of photocatalytic activity is due to the extinction of TiO<sub>2</sub> nanowires under visible irradiation.

In order to get the accurate kinetic data, the rate constants of photodegradation of MB were calculated according to the following first-order kinetics<sup>31</sup>

$$\ln\left(\frac{C}{C_0}\right) = -kt$$

Where C<sub>0</sub> is the initial concentration of the MB solution, C is the concentration of the MB solution, *k* is a rate constant and *t* is the reaction time. After a simple calculation, the values of *k* are 0.025, 0.055 and 0.032 min<sup>-1</sup> for sample Ag(1)-0.05 M WO<sub>3</sub>-TWS, Ag(3)-0.05 M WO<sub>3</sub>-TWS and Ag(5)-0.05 M WO<sub>3</sub>-TWS under simulated solar irradiation, and 0.0078, 0.012 and 0.009 under visible irradiation, respectively. The results indicate that Ag(3)-0.05 M WO<sub>3</sub>-TWS nanocomposites have better photocatalytic activities. Similarly, the values of *k* are 0.006, 0.007, 0.017 and 0.014 for pure TiO<sub>2</sub> nanowires, 0.01M WO<sub>3</sub>-TWS, 0.05M WO<sub>3</sub>-TWS and 0.1M WO<sub>3</sub>-TWS under simulated solar irradiation, and 0.0003, 0.001, 0.0046 and 0.0049 min<sup>-1</sup> under simulated visible irradiation, respectively. The results indicate that 0.05M WO<sub>3</sub>-TWS nanocomposites have better photocatalytic activities under simulated solar irradiation and 0.1M WO<sub>3</sub>-TWS nanocomposites have better photocatalytic activities under simulated visible irradiation.

Fig. 7 shows the schematic diagram of the enhanced photocatalytic activity for the TiO<sub>2</sub> nanowires decorated with Ag and WO<sub>3</sub> nanoparticles. The coupling between a UV excited semiconductor (TiO<sub>2</sub>) and a visible light excited semiconductor (WO<sub>3</sub>) can effectively enhance the solar energy utilization efficiency, especially in the visible light range. TiO<sub>2</sub> possess higher conduction band and valence band than that of WO<sub>3</sub>. The band configuration induces the transfer of photogenerated electrons from TiO<sub>2</sub> to WO<sub>3</sub> and photogenerated holes from WO<sub>3</sub> to TiO<sub>2</sub>, which makes charge separation more efficient. In addition, the photogenerated electrons in TiO<sub>2</sub> will be transferred to Ag nanoparticles, which play two important roles. One is to produce the absorption band in the visible light range due to the

surface Plasmon resonance and the other is to serve as an electron sink, leading to the efficient separation of the photogenerated electrons and holes pairs and the inhibition of their recombination. Therefore, with the synergetic help of  $\text{WO}_3$  and Ag nanoparticles, more photogenerated electrons and holes pairs can be produced, participate in the photodegradation reaction and enhance the photocatalytic activity dramatically. However, excessive Ag nanoparticles will cover more  $\text{TiO}_2$  surface area, increase the reflection of the incident light, lead to the reduction of the number of photons absorbed by  $\text{TiO}_2$  and hence decrease the number of electrons and holes generated by irradiation. Furthermore, excessive Ag nanoparticles not only hinder the adsorption of the dye molecules onto the surface of the composites, but also act as recombination centers for photogenerated electrons and holes, all of which may be responsible for the decrease of the photocatalytic activity for the case of exceeding Ag loading.<sup>29, 32, 33</sup>

The recyclability and ease of collection for the photocatalysts are very important in practical application.<sup>34</sup> Fig. 8 shows the photographs and photodegradation percentage of a typical sample Ag(3)-0.05 M  $\text{WO}_3$ -TWS for recycled methyl orange reduction. First, a piece of sample Ag(3)-0.05 M  $\text{WO}_3$ -TWS was dipped into beaker 1 with 25 ml methyl orange solution (15 mg/l) (Fig. 8a). After 90 min irradiation, the solution in beaker 1 changed from orange to colorless (Fig. 8b). Then, the photocatalysts were taken away from beaker 1 and put into beaker 2 for the second photodegradation (Fig. 8c). Similarly, the solution in beaker 2 became transparent after 90 min irradiation (Fig. 8d). On the basis of ICP-AES (inductively coupled plasma atomic emission spectrometer) analysis, the solution did not contain any second pollution after the reaction. Fig. 8e shows the cycling experiment of the as-prepared photocatalysts for methyl orange degradation using sample Ag(3)-0.05 M  $\text{WO}_3$ -TWS. The degradation percentage remained to be 98.7% after 7 cycles, and 95.6% after 10 cycles. Evidently, the photocatalytic activity toward methyl orange degradation does not change much after each cycle, revealing the excellent cycling stability of the as-prepared photocatalyst composites.

#### 4. Conclusions

In summary,  $\text{WO}_3$ -TWS on the Ti foils were prepared using simple hydrothermal

treatment, wet impregnation and annealing treatment. Ag nanoparticles were deposited on the obtained WO<sub>3</sub>-TWS surfaces by simple SILAR technique. The deposited Ag and WO<sub>3</sub> particles on the surface of the TiO<sub>2</sub> nanowires can efficiently extend the scope of absorption spectrum and greatly enhance the photocatalytic activity in comparison with that of pure TiO<sub>2</sub> nanowires under simulated solar irradiation and visible irradiation. In addition, the as-prepared photocatalyst composites also exhibited excellent long-time recyclable ability for the organic pollutants degradation.

### Acknowledgment

This work was financed by the 211 project of Anhui University, National Natural Science Foundation of China (11374013, 61290301, 51072001, 51272001 and 21374108), Research Fund for the Doctoral Program of Higher Education of China (20133401110002 and 20133402120019), Higher Educational Natural Science Foundation of Anhui Province (KJ2012A007, KJ2012A083).

### References

- [1] S. M. Chin, E. Park, M. Kim, J.S. Jurng, *Powder Technol.*, 2010, **201**, 171-176.
- [2] A. M. Hu, X. Zhang, K. D. Oakes, Y. N. Zhou, M. R. Servos, *J. Hazard. Mater.*, 2011, **189**, 278-285.
- [3] Q. Y. Wang, X. C. Yang, D. Liu, J. F. Zhao, *J. Alloys Comp.*, 2012, **527**, 106-109.
- [4] Y. K. Lai, H. F. Zhuang, K. P. Xie, D. G. Gong, Y. X. Tang, L. Sun, C. J. Lin, Z. Chen, *New J. Chem.*, 2010, **34**, 1335-1340.
- [5] A. A. Ismail, D. W. Bahnemann, *Green Chem.*, 2011, **13**, 428-435.
- [6] X. F. You, F. Chen, J. L. Zhang, *Catal. Lett.*, 2005, **102**, 246-250.
- [7] H. Guo, W. Wang, L. X. Liu, Y. B. He, C. P. Li, Y. P. Wang, *Green Chem.*, 2013, **15**, 2810-2816.
- [8] R. Dagherir, P. Drogui, D. Robert, *Ind. Eng. Chem. Res.*, 2013, **52**, 3581-3599.
- [9] L. Liu, Z. Y. Liu, H. W. Bai, D. D. Sun, *Water Res.*, 2012, **46**, 1101-112.
- [10] J. K. Yang, X. T. Zhang, H. Liu, C. H. Wang, S. P. Liu, P. P. Sun, L. L. Wang, Y. H. Liu, *Catal. Today*, 2013, **201**, 195-202.
- [11] Y. Liu, J. C. Hu, J. L. Li, *J. Alloys Comp.*, 2011, **509**, 5152.
- [12] W. Ho, J. C. Yu, S. Lee, *Electrochem. Commun.*, 2006, 1115-117.
- [13] W. B. Liang, T. L. Church, A. T. Harris, *Green Chem.*, 2012, **14**, 968-975.
- [14] C. He, D. Shu, M. H. Su, D. H. Xia, M. A. Asi, L. Lin, Y. Xiong, *Desalination*, 2010, **253**, 88-93.
- [15] H. X. Li, Z. F. Bian, J. Zhu, Y. N. Huo, H. Li, Y. F. Lu, *J. Am. Chem. Soc.*, 2007, **129**, 4538-4539.
- [16] Y. N. Huo, X. L. Yang, J. Zhu, H. X. Li, *Appl. Catal. B: Environ.*, 2011, **106**, 69-75.
- [17] H. Chen, S. Chen, X. Quan, H. T. Yu, H. M. Zhao, Y. B. Zhang, *J. Phys. Chem. C*, 2008, **112**, 9285-9290.
- [18] Y. J. Wang, Q. S. Wang, X. Y. Zhan, F. M. Wang, M. Safdar, J. He, *Nanoscale*, 2013, **5**, 8326-8339.
- [19] K. Lu, J. Li, X. X. Qing, W. Z. Li, Q. Y. Chen, *J. Hazard. Mater.*, 2011, **189**, 329-335.

- [20] K. I. Liu, Y. C. Hsueh, C. Y. Su, T. P. Perng, *Int. J. Hydrogen Energy*, 2013, **38**, 7750-7755.
- [21] F. Riboni, L. G. Bettini, D. W. Bahnemann, E. Selli, *Catal. Today*, 2013, **209**, 28-34.
- [22] L. Shang, B. J. Li, W. J. Dong, B. Y. Chen, C. R. Li, W. H. Tang, G. Wang, J. Wu, Y. B. Ying, *J. Hazard. Mater.*, 2010, **178**, 1109-1114.
- [23] Q. Y. Wang, X. C. Yang, D. Liu, J. F. Zhao, *J. Alloys Comp.*, 2012, **527**, 106-111.
- [24] L. L. Ren, Y. P. Zen, D. L. Jiang, *Cata. Commun.*, 2009, **10**, 645-649.
- [25] R. Vinu, G. Madras, *Appl. Catal. A-Gen.*, 2009, **366**, 130-140.
- [26] L. Sun, J. Li, C. L. Wang, S. F. Li, Y. K. Lai, H. B. Chen, C. J. Lin, *J. Hazard. Mater.*, 2009, **171**, 1045-1050.
- [27] F. Petronella, S. Diomede, E. Fanizza, G. Mascolo, T. Sibillano, A. Agostiano, M. L. Curri, R. Comparelli, *Chemosphere*, 2013, **91**, 941-947.
- [28] G. M. Guo, B. B. Yu, P. Yu, X. Chen, *Talanta*, 2009, **79**, 570-575.
- [29] C. W. Lai, S. Sreekantan, *Electrochim. Acta*, 2013, **87**, 294-302.
- [30] V. Vamathevan, R. Amal, D. Beydoun, G. Low, S. McEvoy, *J. Photochem. Photobiol. A.*, 2002, **148**, 233-245.
- [31] P. Dai, L. L. Zhang, G. Li, Z. Q. Sun, X. S. Liu, M. Z. Wu, *Mater. Res. Bull.*, 2014, **50**, 440-445.
- [32] B. Subash, B. Krishnakumar, B. Sreedhar, M. Swaminathan, M. Shanthi, *Superlattice. Microst.*, 2013, **54**, 155-171.
- [33] X. F. Yang, J. L. Qin, Y. Li, R. X. Zhang, H. Tang, *J. Hazard. Mater.*, 2013, **261**, 342-350.
- [34] R. Li, P. Zhang, Y. M. Huang, C. L. Chen, Q. W. Chen, *ACS Appl. Mater. Interfaces*, 2013, **23**, 12695-12700.

**Captions:**

Fig. 1. XRD patterns of (a)  $\text{WO}_3$ -TWS samples and (b)  $\text{Ag}(i)$ -0.05M  $\text{WO}_3$ -TWS ( $i=1, 3, 5$ ).

Fig. 2. XPS spectra of the (a) Ti2p, (b) O1s, (c) W4f, and (d) Ag3d regions for  $\text{TiO}_2$  nanowires, 0.05 M  $\text{WO}_3$ -TWS and  $\text{Ag}(3)$ -0.05 M  $\text{WO}_3$ -TWS.

Fig. 3. SEM images of  $\text{TiO}_2$  nanowires, 0.05 M  $\text{WO}_3$ -TWS,  $\text{Ag}(i)$ -0.05 M  $\text{WO}_3$ -TWS ( $i=1,3,5$ )(a-e) and EDS spectra of 0.05 M  $\text{WO}_3$ -TWS,  $\text{Ag}(3)$ -0.05 M  $\text{WO}_3$ -TWS (f).

Fig.4. TEM and HRTEM images of 0.05 M  $\text{WO}_3$ -TWS(a,b) and  $\text{Ag}(3)$ -0.05 M  $\text{WO}_3$ -TWS (c,d,e).

Fig. 5. UV-vis absorption spectra of (a)  $\text{TiO}_2$  nanowires, 0.01 M  $\text{WO}_3$ -TWS, 0.05 M  $\text{WO}_3$ -TWS, 0.1 M  $\text{WO}_3$ -TWS; (b)  $\text{Ag}(i)$ -0.05 M  $\text{WO}_3$ -TWS ( $i=1,3,5$ ).

Fig. 6. Photodegradation percentages of (a)  $\text{TiO}_2$  nanowires, 0.01 M  $\text{WO}_3$ -TWS, 0.05 M  $\text{WO}_3$ -TWS for methyl orange solution under simulated solar irradiation; (b)  $\text{TiO}_2$  nanowires, 0.01 M  $\text{WO}_3$ -TWS, 0.05 M  $\text{WO}_3$ -TWS for methyl orange solution under visible irradiation obtained using a 420 nm cutoff filter; (c)  $\text{Ag}(i)$ -0.05 M  $\text{WO}_3$ -TWS ( $i=1,3,5$ ) for methyl orange solution under simulated solar irradiation; (d)  $\text{TiO}_2$  nanowires, 0.01 M  $\text{WO}_3$ -TWS, 0.05 M  $\text{WO}_3$ -TWS for methyl orange solution under visible irradiation obtained using a 420 nm cutoff filter.

Fig. 7. Schematic diagram of charge carrier separation in the photoexcited  $\text{Ag-WO}_3/\text{TiO}_2$ .

Fig. 8. Schematic diagram of separation and reuse of photocatalysts (a-d) and time-dependent photocatalytic degradation percentage of the cycling experiments for methyl orange solution using sample  $\text{Ag}(3)$ -0.05 M  $\text{WO}_3$ -TWS (e).

Fig. 1.

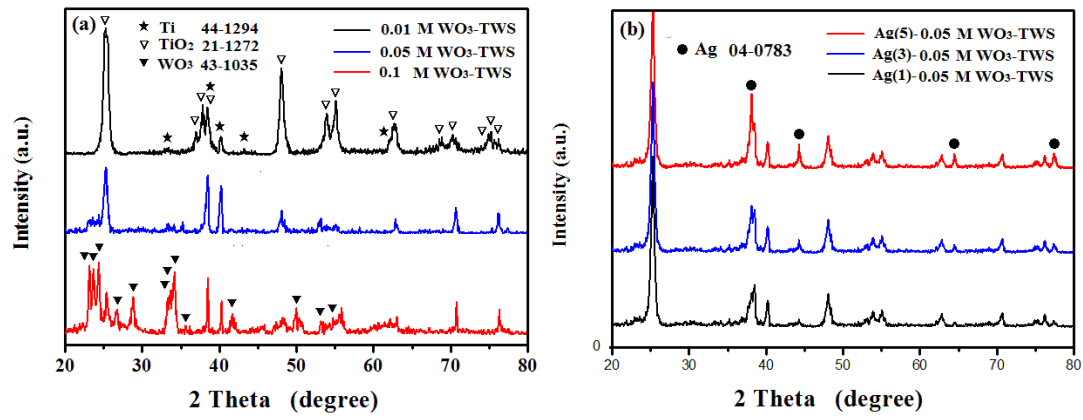


Fig. 2.

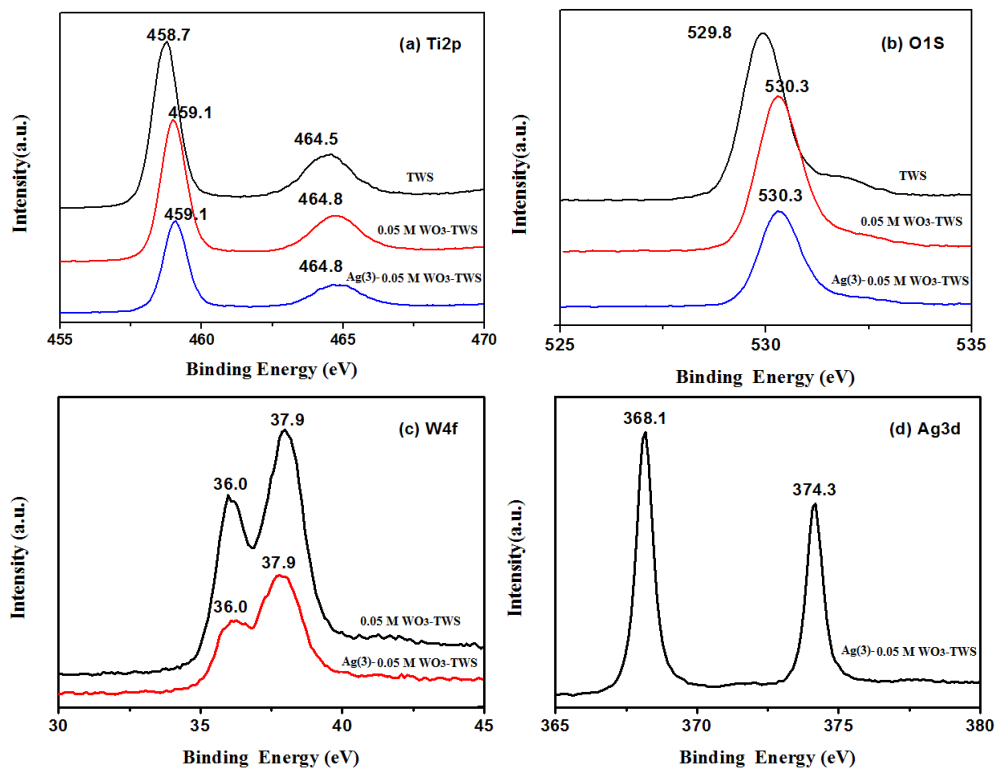


Fig. 3.

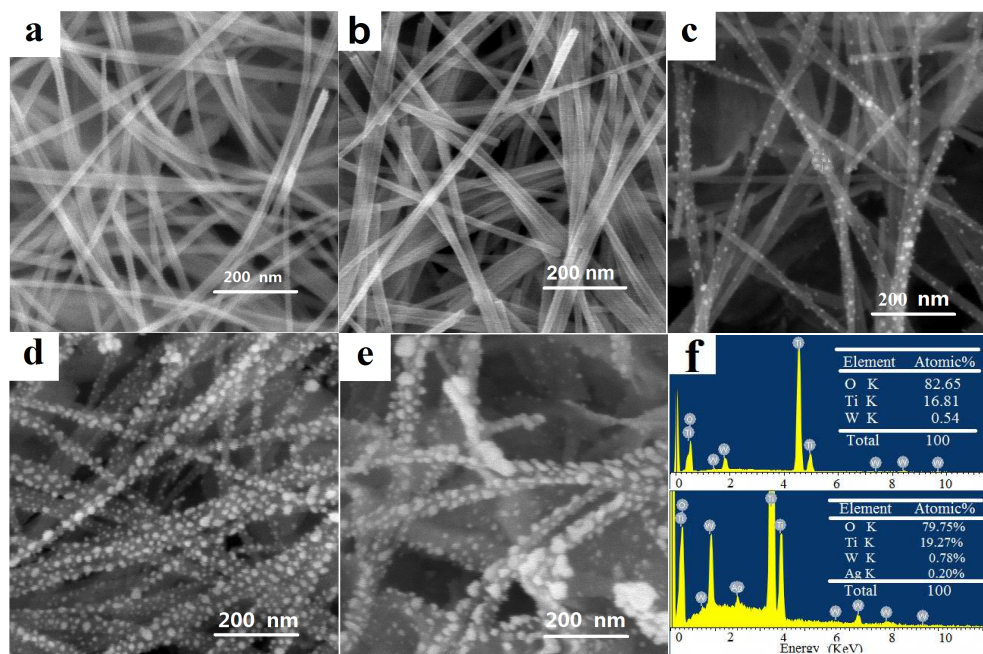


Fig. 4.

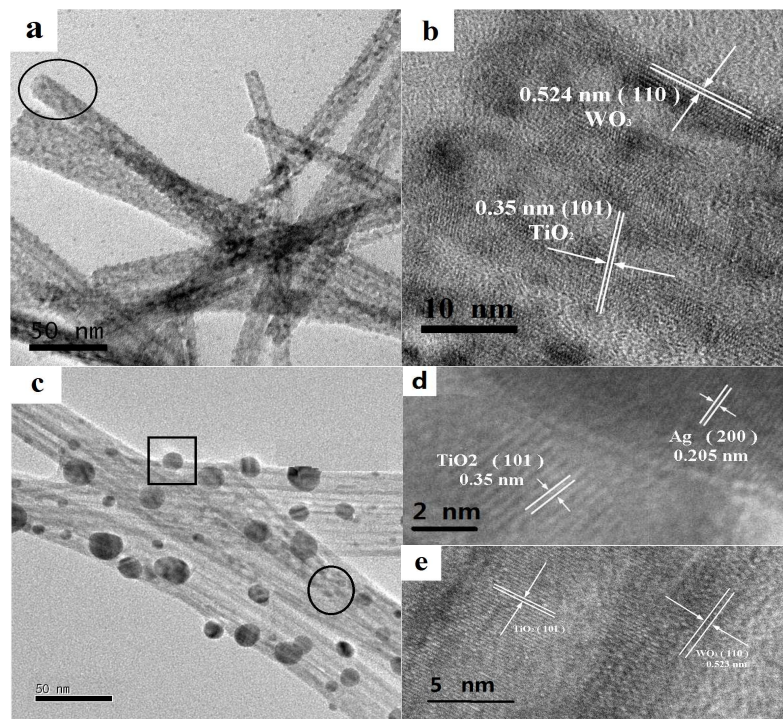


Fig. 5.

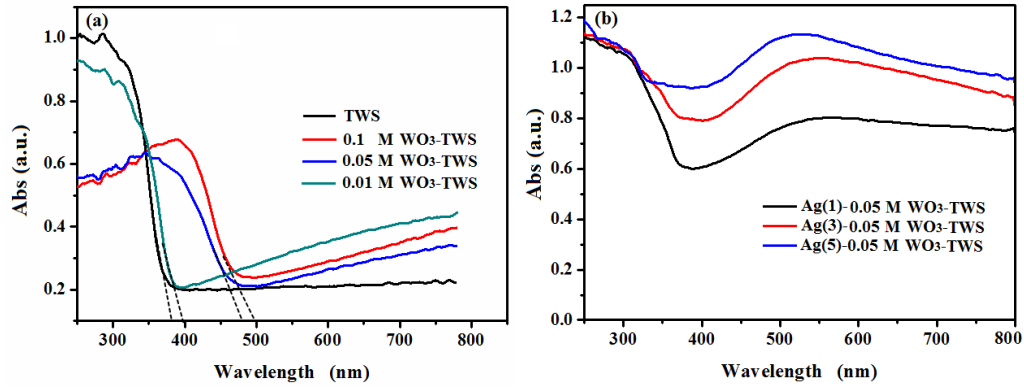


Fig. 6.

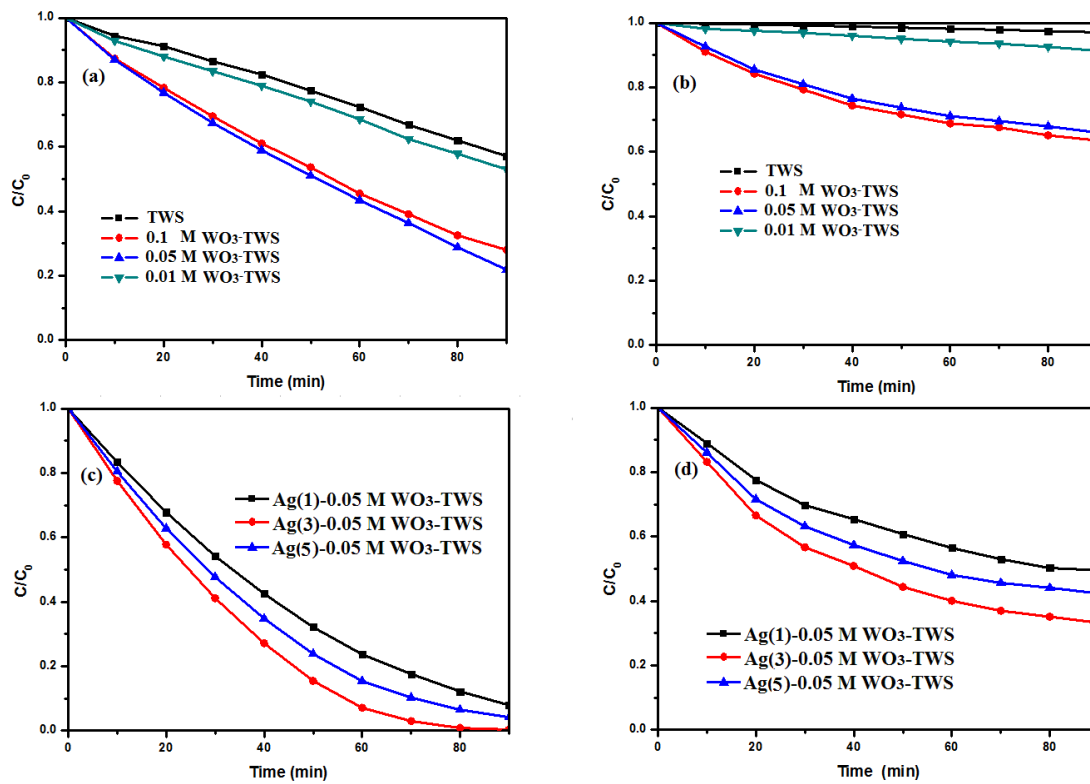


Fig. 7.

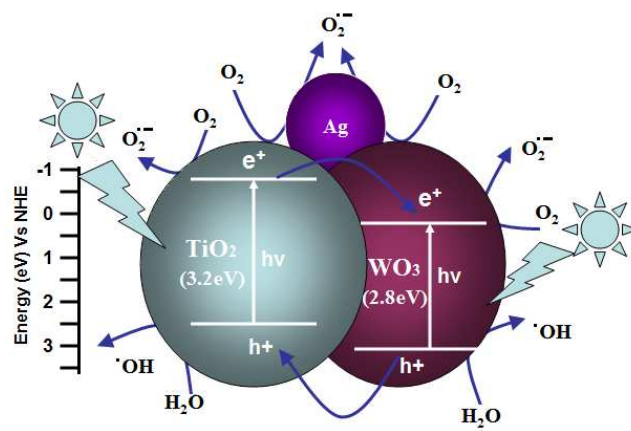


Fig. 8.

